# CrystEngComm



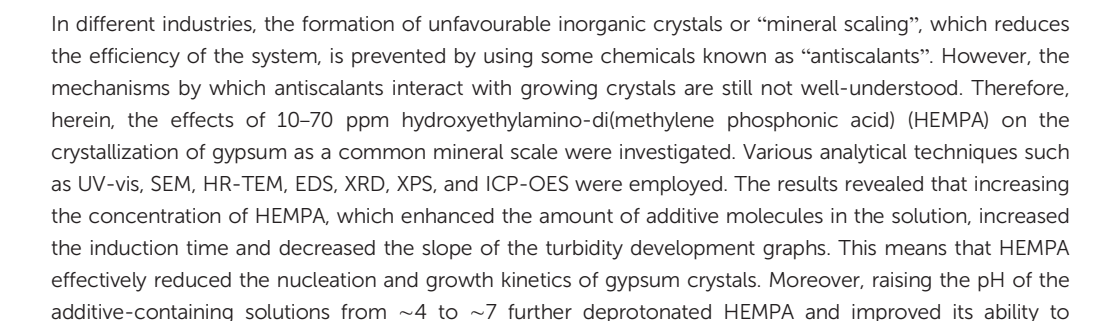
## **PAPER**



Cite this: CrystEngComm, 2023, 25, 935

## Investigating the potential of hydroxyethylaminodi(methylene phosphonic acid) in inhibiting gypsum crystallization†

Taher Rabizadeh (10)



hinder gypsum formation. Hence, at pH  $\sim$  7, no gypsum crystals precipitated except in the 10 ppm

HEMPA-dosed electrolyte. Furthermore, the solids formed in the blank system were thin, large, and

elongated along the c direction compared to the tiny particles produced with 70 ppm HEMPA (at pH  $\sim$  4). The findings also indicated that at the appropriate HEMPA-concentration and solution pH, HEMPA

significantly inhibits gypsum crystallization through various mechanisms including chelation of crystal-

forming ions in the solution, surface adsorption, and structural incorporation.

Received 22nd August 2022, Accepted 21st December 2022

DOI: 10.1039/d2ce01156e

by temperature fluctuations, the degree of supersaturation, and the presence of impurities. <sup>16,17</sup> Therefore, much effort is made to study the crystallization pathway of this mineral and inhibit its precipitation.

According to the literature, acid washing and/or mechanical cleaning are the techniques commonly used to remove precipitated mineral scales. However, these techniques have disadvantages such as corrosion or surface damage. Hence, hindering mineral scaling by dosing chemicals known as "antiscalants" into the system is recommended. 21,22

Until now, many industrial antiscalants have been produced and among the effective ones are those with phosphonate, carboxylate, and sulfonate functional groups in their molecular structures. For example, it was observed that sodium polyaspartate and 1-hydroxyethylidine 1,1-diphosphonic acid (HEDP) prevented barite and calcite precipitation, respectively.

In the case of gypsum scaling, it has been reported that the presence of 2 ppm poly(acrylic acid) inhibits the gypsum formation process by 94%.<sup>27</sup> Akyol *et al.* also reported that increasing the molecular weight of carboxymethyl inulin from 3000 to 6500 effectively reduced the amount of gypsum crystals that precipitated in the system.<sup>28</sup> The gypsum

## rsc.li/crystengcomm

1. Introduction

In various industries, such as petroleum, hydrometallurgy, water purification, and geothermal energy production, the presence of supersaturated solutions results in the nucleation and growth of some sparingly soluble minerals. During this unfavourable phenomenon which is called "mineral scaling", the pipelines and membranes get clogged and sometimes corroded. Therefore, mineral scale formation reduces the lifetime of industrial facilities and leads to increased maintenance or replacement costs.

There are various types of mineral scales but the common ones are calcite,  $^9$  barite,  $^{10,11}$  struvite,  $^{12}$  silica,  $^{13}$  and gypsum.  $^{14}$  Gypsum or calcium sulfate dihydrate (CaSO $_4$ ·2H $_2$ O) is a crystalline phase in the CaSO $_4$ -H $_2$ O system and its formation is important from the natural geochemical and industrial points of view.  $^{15}$  However, gypsum precipitation, which is usually encountered in water desalination plants, is affected

Department of Materials Engineering, Faculty of Mechanical Engineering,
University of Tabriz, 51666-16471, Tabriz, Iran. E-mail: t.rabizadeh@tabrizu.ac.ir
† Electronic supplementary information (ESI) available. See DOI: https://doi.org/10.1039/d2ce01156e

antiscaling potential of different aminophosphonates such as aminotris(methylene phosphonic acid) (ATMP) has also been documented.29,30

However, the ability of hydroxyethylamino-di(methylene phosphonic acid) (HEMPA) in preventing gypsum mineral scaling has not yet been investigated. Most importantly, how this additive might interact with gypsum crystals and affect their precipitation kinetics is still unclear.

To address these questions, gypsum crystallization was probed in the absence and presence of HEMPA. The effects of the additive concentration and the solution pH on the nucleation and growth kinetics, morphology, and gypsum/ HEMPA interactions were evaluated by various analytical techniques. Our findings revealed that HEMPA, even at ppm levels, delayed gypsum formation via both surface adsorption and structural incorporation which affected the morphology of the synthesized crystals.

## 2. Experimental methods

To produce calcium sulfate dihydrate (gypsum) crystals, 250 ml of a 0.15 M CaCl<sub>2</sub>·2H<sub>2</sub>O (ACS reagent; Sigma-Aldrich) solution was added to 250 ml of a 0.15 M Na<sub>2</sub>SO<sub>4</sub> (ACS reagent; Sigma-Aldrich) solution at room temperature. The obtained supersaturated solution was stirred continuously for 240 min before vacuum filtering the final products.

The tested additive was hydroxyethylamino-di(methylene phosphonic acid) (HEMPA; C<sub>4</sub>H<sub>13</sub>NO<sub>7</sub>P<sub>2</sub>; THWATER Co. Ltd.) and its molecular structure is depicted in Fig. 1. The gypsum crystallization process in the presence of HEMPA was conducted by dosing 20 ppm, 60 ppm, 100 ppm or 140 ppm of this compound into the sodium sulfate solution before the addition of an additive-free calcium chloride solution. Hence, the initial additive concentration in the gypsum formation solution varied in the range of 10-70 ppm. Further, the role of pH in the gypsum precipitation process in the absence and presence of HEMPA was evaluated by adjusting the pH of both calcium and sulfate solutions to ~4 or ~7 before mixing. For pH adjustment, a few milliliters of NaOH and/or HCl solutions was used.

The nucleation and growth kinetics of calcium sulfate dihydrate crystals in the absence and presence of HEMPA were monitored using a UV-vis instrument (Jenway 7305). In

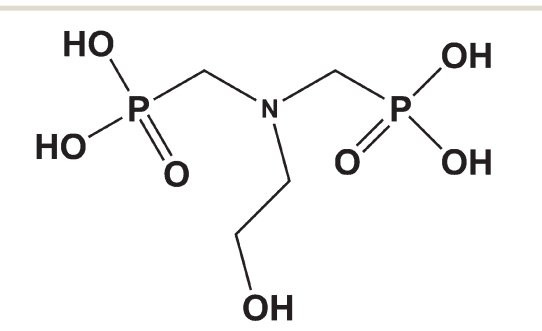


Fig. 1 Molecular structure of hydroxyethylamino-di(methylene phosphonic acid).

this regard, at appropriate time intervals, the absorbance of 2.5 mL aliquots pipetted from the crystallization solutions was measured at  $\lambda$  = 520 nm and 21 °C. Normalizing the recorded data with respect to the maximum absorbance value obtained in the absence of the additive and plotting them (in %) over time yielded the turbidity development curves which were used as a proxy to evaluate the crystallization kinetics. These procedures were repeated three times.

The phase and morphology of the crystals obtained from the blank and the HEMPA-containing solutions were evaluated utilizing X-ray diffraction (XRD; Bruker D8 diffractometer; CuKα1), field emission gun scanning electron microscopy (FEG-SEM, FEI Quanta 650, 5 kV) and field emission gun electron source transmission electron microscopy (TEM; FEI Tecnai G2 F20 X-Twin; 200 kV).

A high-resolution TEM equipped with a Gatan Tridiem energy filter, a Fischione high-angle annular dark field detector, and an energy dispersive X-ray analyzer (EDS) was utilized for bright- and dark-field imaging, together with chemical composition analyses. A diamond saw microtome (Leica Saw SP1600) was also used to produce ultrathin sections of the resin-embedded gypsum end-products.

The amounts of calcium and HEMPA consumed during gypsum formation were assessed by measuring the concentrations of Ca<sup>2+</sup> and P in the aliquots taken from the blank or the HEMPA-amended solutions 10 seconds (initial concentration) and 240 min (final concentration) after the onset of supersaturation. In some experiments, the concentration of HEMPA during the gypsum crystallization process was also determined. It should be noted that based on the molecular weight of HEMPA, the measured concentration of P (in ppm) was converted to the amount of HEMPA (in ppm) present in the solution. The aqueous elemental analyses were performed using an inductively coupled plasma optical emission spectrometer (ICP-OES; Thermo Scientific iCAP 7400).

To determine whether HEMPA had any interactions with the formed gypsum crystals, the top layers of the obtained solids were probed by X-ray photoelectron spectroscopy (XPS; Kratos Axis Ultra-DLD spectrometer; detection limit: 0.1 at%; base pressure:  $ca. 6 \times 10^{-7}$  Pa). High-resolution XPS scans were obtained with a monochromatic aluminum  $K_{\alpha}$  X-ray source (144 W) and pass energies of 40 eV. The C (1s) signal detected at a binding energy of 284.8 eV was also used as a charge reference. In addition, the amount of the elements (in at%) was defined using CasaXPS™ software (Version 2.3.15).

#### 3. Results

The turbidity changes versus time were plotted to evaluate the gypsum crystallization kinetics in the absence and presence of HEMPA at two pH values of ~4 or ~7 (Fig. 2 and 3). For further clarity, the corresponding "absorbance vs. time" plots were also presented (Fig. S1 and S2†).

At pH  $\sim$  4, it can be seen that in the HEMPA-free solution, the turbidity curve deviated from the baseline after  $\sim$ 2  $\pm$  1

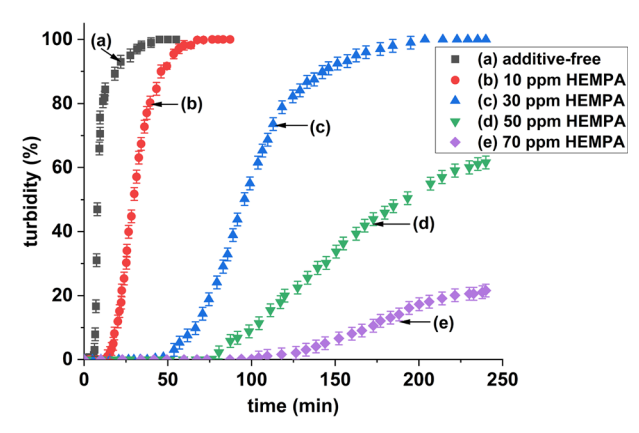


Fig. 2 Turbidity vs. time plots obtained in the absence and presence of different concentrations of HEMPA at pH ~ 4. Note that the corresponding absorbance vs. time plots are reported in the supporting document as Fig. S1.†

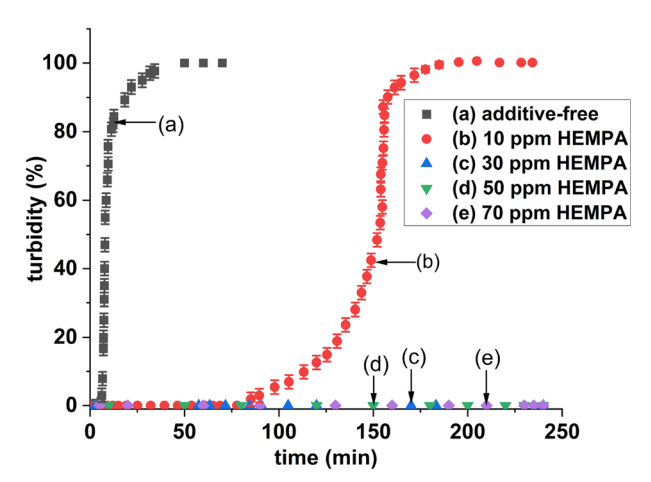


Fig. 3 Turbidity vs. time plots obtained in the absence and presence of different concentrations of HEMPA at pH  $\sim$  7. Note that the corresponding absorbance vs. time plots are reported in the supporting document as Fig. S2.†

min which is known as the induction time. Moreover, after a sharp increase, the turbidity reached 100% within  $\sim$ 30  $\pm$  1 min (Fig. 2). In contrast, the presence of HEMPA affected both the induction time and the slope of the turbidity development graphs. It is obvious that dissolving 10 ppm HEMPA in the crystallization solution increased the induction time to  $\sim$ 14  $\pm$  2 min, whilst the presence of 30 ppm, 50 ppm or 70 ppm HEMPA yielded the induction times of  $\sim$ 27 ± 2 min,  $\sim$ 75 ± 3 min, or 100 ± 5 min, respectively. Meanwhile, the slope of the linear part of the turbidity development plots decreased from  $25 \pm 0.1$  (% min<sup>-1</sup>) in the additive-free system to  $4 \pm 0.1$ ,  $1.5 \pm 0.1$ ,  $0.5 \pm 0.1$  or  $0.2 \pm 0.1$ (% min<sup>-1</sup>) in the 10 ppm, 30 ppm, 50 ppm, or 70 ppm HEMPA-containing solutions, respectively. It is also notable that the turbidity plots just reached 100% with 10 ppm HEMPA (after ~50 min) and 30 ppm HEMPA (after ~85 min). Meanwhile, a maximum turbidity of 80% or 30% was

obtained in the 50 ppm or 70 ppm HEMPA-dosed electrolyte, respectively.

At pH  $\sim$  7, the graph obtained from the blank solution was almost similar to the one plotted at pH  $\sim$  4 (Fig. 3). However, in the presence of HEMPA, the induction time was just recorded in the 10 ppm HEMPA amended system. With 10 ppm HEMPA (at pH  $\sim$  7), the induction time was  $\sim$ 60 min. After this period of time, the turbidity plot developed exponentially for the next 90 min until it reached 55%. At this point, the corresponding plot abruptly increased with a slope similar to the slope of the turbidity changes in the HEMPA-free solution and subsequently levelled off after 10 min (totally  $\sim$ 195 min from the onset of supersaturation).

To further evaluate the antiscaling performance of HEMPA, the concentration of this additive was measured ~10 seconds (initial concentration) and 240 min (endconcentration) after the onset of supersaturation. As indicated in Fig. 4, at pH ~ 4, the end-concentration of HEMPA was  $\sim 2$  ppm,  $\sim 12$  ppm,  $\sim 27$  ppm or  $\sim 58$  ppm when 10 ppm, 30 ppm, 50 ppm or 70 ppm HEMPA was initially dissolved in the solution, respectively. However, at pH  $\sim$  7, HEMPA was almost removed from the 10 ppm additivecontaining solution (yielding an end-concentration of ~0.7 ppm) whilst its concentration in the 30 ppm, 50 ppm, or 70 ppm amended solutions remained constant.

To obtain an insight into the depletion pathway of 10 ppm HEMPA during gypsum formation at pH ~ 7, the amount of this additive in the solution was monitored for 240 min (Fig. 5). It is apparent that after the induction time the concentration of HEMPA in the solution gradually decreased. Therefore, the turbidity and the HEMPA concentration plots almost mirrored each other.

The effects of HEMPA on the gypsum crystallization process were also evaluated by measuring the concentration of Ca<sup>2+</sup> in the blank and in the HEMPA-containing electrolytes after 240 min (Table 1). At pH ~ 4, the concentration of Ca<sup>2+</sup> in the additive-free solution decreased from the initial concentration of ~75 mM to ~21 mM. Meanwhile, in the presence of 10 ppm, 30 ppm, 50 ppm, or

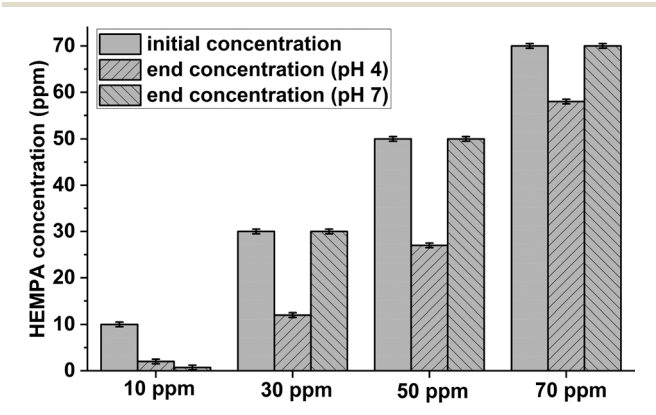


Fig. 4 The initial and end concentrations of 10 ppm, 30 ppm, 50 ppm and 70 ppm of HEMPA in the gypsum formation solutions measured at pH  $\sim$  4 and  $\sim$ 7.

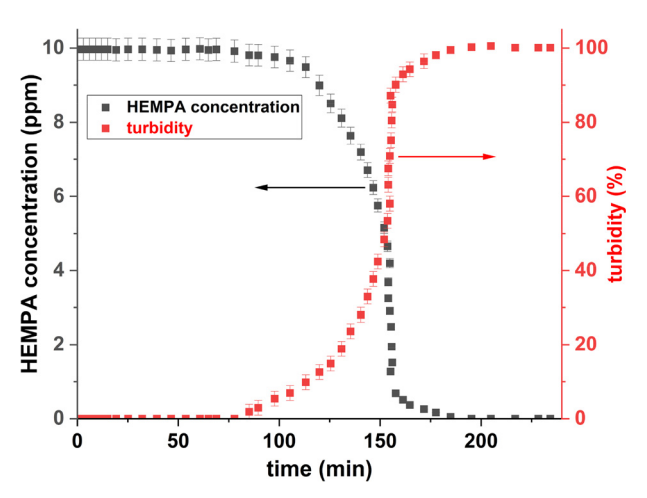


Fig. 5 Changes in the turbidity and the amount of 10 ppm HEMPA in the gypsum formation solution measured at pH  $\sim$  7.

Table 1 The amount of calcium ion (in mM) remained in blank or the HEMPA containing systems at different pH values

	Additive-free	10 ppm	30 ppm	50 ppm	70 ppm
pH ~ 4	21 ± 1.4	$25 \pm 1.3$	40 ± 1.3	51 ± 1.5	60 ± 1.5
pH ~ 7	23 ± 1.3	$34 \pm 1.3$	0	0	0

70 ppm HEMPA, ~25 mM, ~40 mM, ~51 mM or ~60 mM Ca<sup>2+</sup> remained in the solution, respectively. In addition, at pH ~ 7, the unused amount of calcium ions in the plain gypsum formation solution was ~23 mM which was almost similar to the measured  $Ca^{2+}$  end-concentration at pH  $\sim 4$ . Besides, ~34 mM Ca<sup>2+</sup> was not consumed in the 10 ppm HEMPA amended solution whilst with 30 ppm, 50 ppm or 70 ppm HEMPA the initial concentration and the endconcentration of Ca<sup>2+</sup> were equal.

The top layers of gypsum crystals filtered from the solutions without and with HEMPA at different pH values were characterized by XPS (Table 2). As an example, the XPS spectrum for the gypsum crystals gathered from the 30 ppm HEMPA amended solution at pH  $\sim$  4 is presented in Fig. 6. In this figure, the Ca 2p, S 2p, and O 1s peaks occurred at binding energies of 347.31 eV, 168.31 eV, and 531.31 eV, respectively, which are related to gypsum crystals. The Na 1s, Cl 2p peaks detected at binding energies of 1071.31 eV and

Table 2 XPS data (in at%) related to gypsum crystals synthesized in the absence and presence of HEMPA

	Ca	S	О	Na	Cl	P	$\mathbf{C}^a$
Additive-free	12.3	12.5	59.9	0.2	0.1	_	15
10 ppm-pH $\sim 4$	12.2	12.7	59.7	0.2	0.1	_	15.1
10 ppm−pH ~ 7	12.3	12.7	59.5	0.2	0.1	0.3	14.9
30 ppm-pH $\sim 4$	12.2	12.7	59.6	0.2	0.1	0.4	14.8
50 ppm-pH $\sim 4$	12.2	12.6	59.7	0.2	0.1	0.5	14.7
70 ppm–pH $\sim 4$	12.2	12.6	59.6	0.2	0.1	0.7	14.6

<sup>&</sup>lt;sup>a</sup> Adventitious carbon.

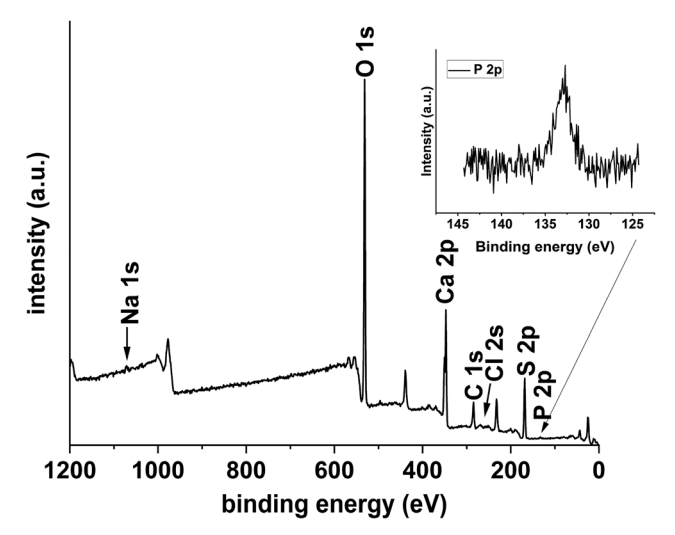


Fig. 6 XPS spectra for gypsum crystals synthesized in the presence of 30 ppm HEMPA at pH  $\sim$  4.

268.31 eV, respectively, are assigned to NaCl already present in the electrolyte. Moreover, the P 2p signal observed at a binding energy of 133.31 eV originates from HEMPA dissolved in the solution.

The morphology of calcium sulfate dihydrate crystals synthesized in the absence and presence of HEMPA was analysed by SEM (Fig. 7). At pH  $\sim$  4, it is evident that without HEMPA, large, thin and elongated crystals were formed (Fig. 7a), which were almost similar to the solids filtered from the additive-free system at pH  $\sim$  7 (Fig. S3†). However, 10 ppm HEMPA made the gypsum crystals slightly smaller and in some cases thicker (Fig. 7b). Significant changes in the morphology of gypsum crystals were observed when 30 ppm, 50 ppm or 70 ppm HEMPA was dissolved in the solution. It is evident that the solids formed in the 30 ppm containing solution were much shorter and thicker than the pure ones (Fig. 7c). In addition, increasing the concentration of HEMPA to 50 ppm resulted in the formation of smaller crystals with irregular shapes (Fig. 7d). Moreover, at 70 ppm HEMPA, very tiny solids were obtained (Fig. 7e).

At pH  $\sim$  7, where the gypsum crystallization just occurred in the 10 ppm HEMPA containing solution, the obtained solids were remarkably smaller than those gathered from the electrolyte containing the same concentration of the additive (at pH  $\sim$  4) (Fig. 7f).

Here, it is noteworthy that the tips of solids filtered from the additive-free solution were almost flat (Fig. 8a) but the presence of 30 ppm HEMPA (at pH  $\sim$  4) yielded crystals with uneven tips (Fig. 8b). The observed morphological changes were further evaluated by XRD measurements (Fig. 9). It is obvious from the XRD patterns that the (020) to (021) peak intensity ratio in the 30 ppm HEMPA containing solution at pH  $\sim 4$  was  $\sim 0.69$  compared to  $\sim 2.6$  calculated for the pure gypsum crystals.

The morphology, size and chemical composition of gypsum crystals synthesized without and with 30 ppm

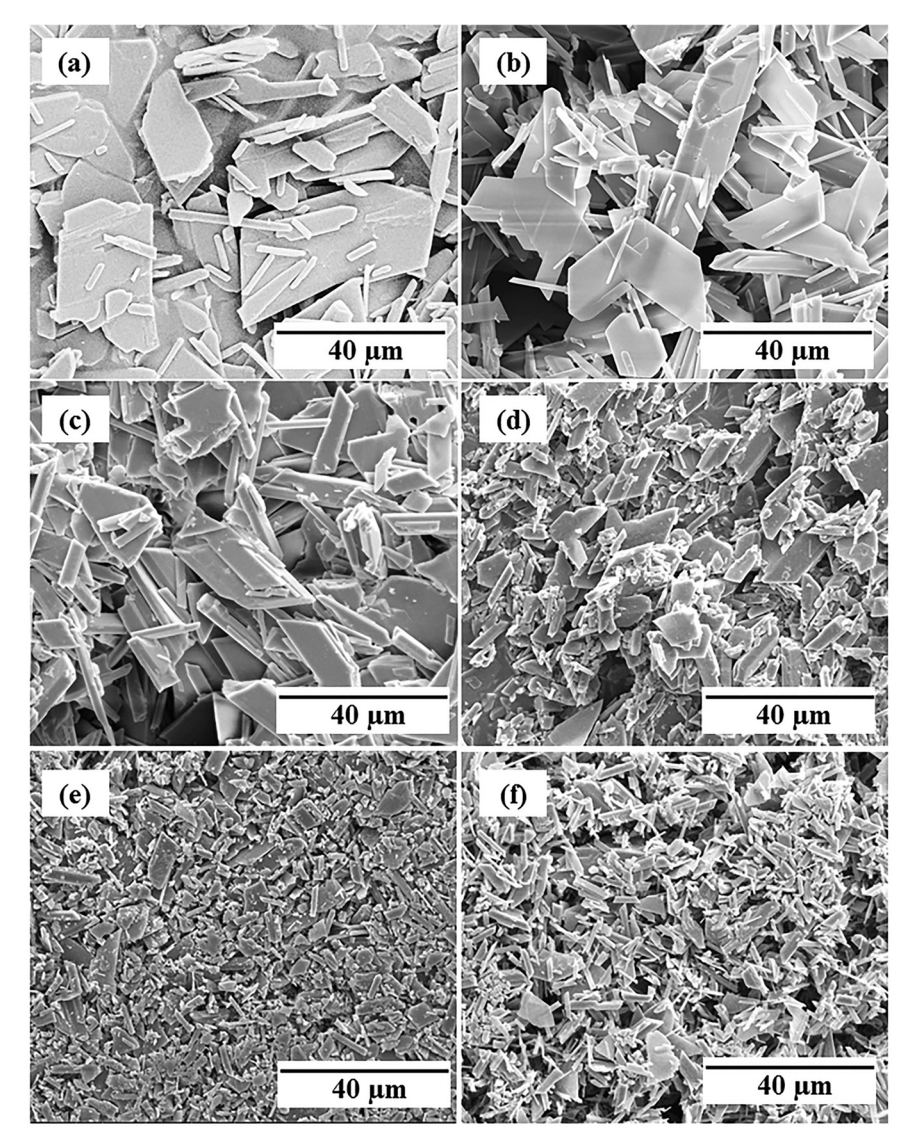


Fig. 7 SEM images of gypsum final products obtained from (a) additive-free at pH  $\sim$  4; (b) 10 ppm HEMPA at pH  $\sim$  4; (c) 30 ppm HEMPA at pH  $\sim$ 4; (d) 50 ppm HEMPA at pH  $\sim$  4; (e) 70 ppm HEMPA at pH  $\sim$  4; (f) 10 ppm HEMPA at pH  $\sim$  7 solutions.

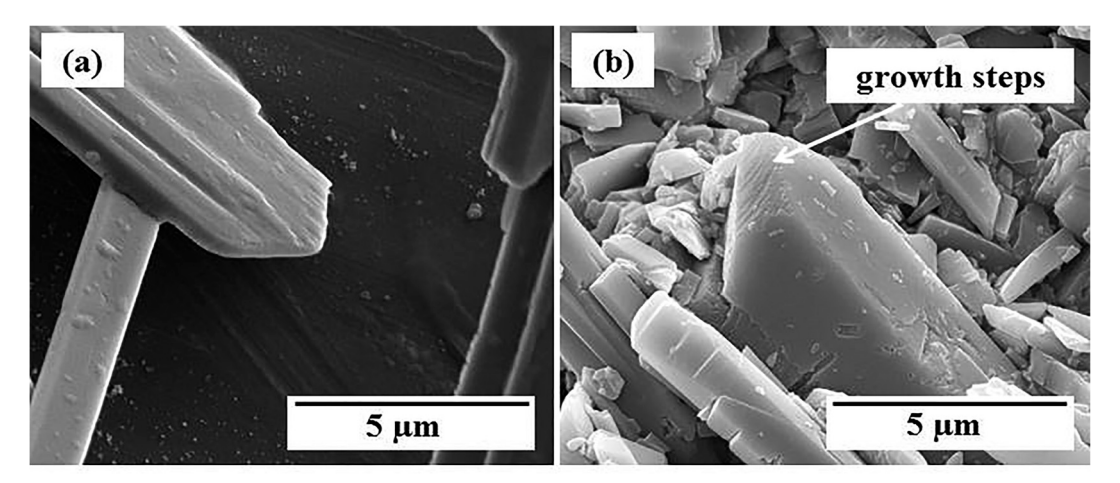


Fig. 8 The tips of gypsum end-products vacuum-filtered from (a) the additive-free; (b) 30 ppm HEMPA solutions (at pH  $\sim$  4).

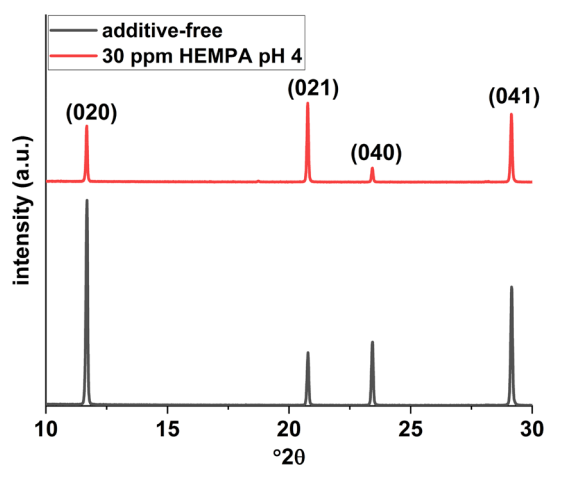


Fig. 9 The variations in the (020) to (021) peak intensity ratio of gypsum crystals produced (a) without and (b) with 30 ppm HEMPA (both at pH  $\sim$  4).

HEMPA were further evaluated by TEM imaging and EDS spectroscopy. According to the results, the crystals precipitated from the additive-free solution had an elongated morphology typical of gypsum (Fig. S4a $\dagger$ ). In contrast, the crystals formed in the presence of 30 ppm HEMPA (at pH  $\sim$  4) were shorter and thicker (Fig. S4b $\dagger$ ). In addition, both

bright-field and dark-field images reveal that the microtommed gypsum crystals produced in the absence and presence of 30 ppm HEMPA (at pH  $\sim$  4) were not homogeneous (Fig. S5 $\dagger$ ). Moreover, the elemental composition analyses revealed the presence of Na and Cl elements in the crystal formed without and with HEMPA whilst P was just detected within the analyzed crystal obtained from the 30 ppm HEMPA containing solution at pH  $\sim$  4 (Fig. 10).

## 4. Discussion

#### 4.1. The role of additives and electrolyte

It is well-documented that the molecular geometry including the backbone chain length, the molecular weight, and the types and number of functional groups together with solution supersaturation and pH are the main factors affecting the efficiency of industrial antiscalants. In addition, there are various mechanisms by which an additive can hinder the crystallization of mineral scales. Some of them are discussed below in relation to our data.

**4.1.1. Chelation/solution pH.** An antiscalant inhibits a crystallization process by sequestrating the crystal forming ions present in the solution (*e.g.*, Ca<sup>2+</sup> in terms of gypsum).<sup>34</sup> This highlights the critical role of the antiscalant

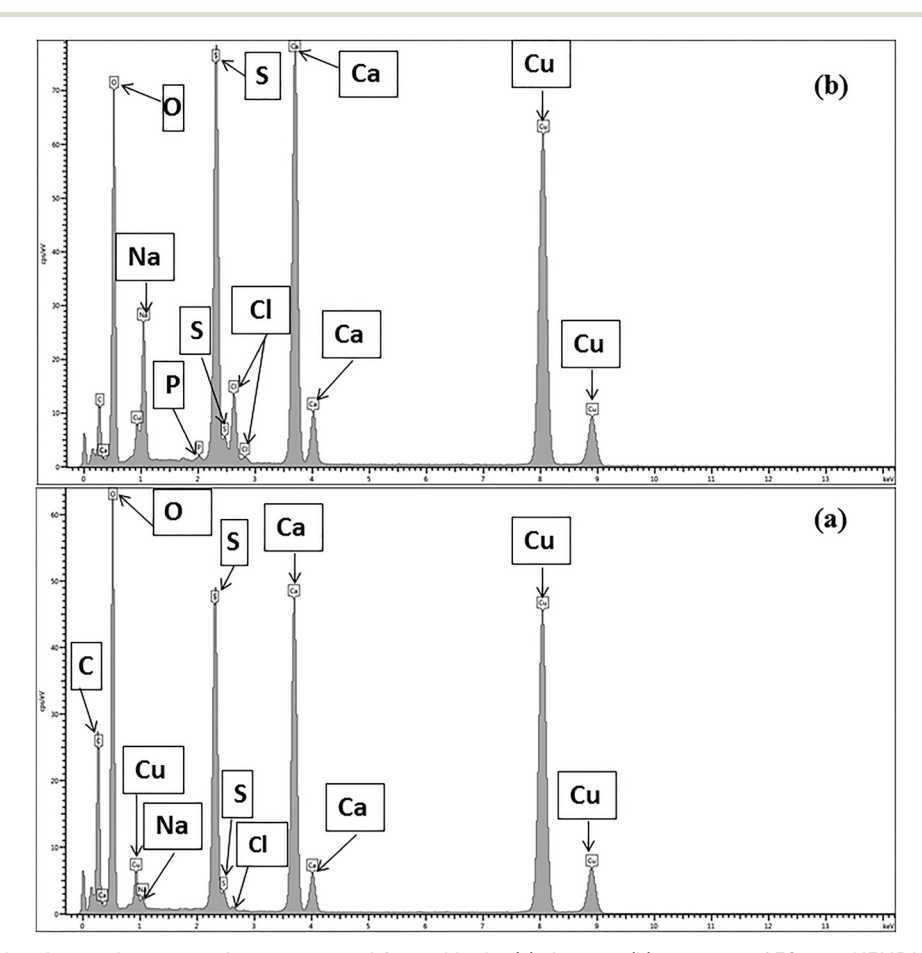


Fig. 10 EDS analysis related to a microtommed gypsum crystal formed in the (a) absence; (b) presence of 30 ppm HEMPA at pH  $\sim$  4.

concentration in the solution. In addition, increasing the pH of the solution deprotonates the dissolved antiscalant and enhances its potential to form strong complexes with the scale forming cations in the electrolyte. 35,36 Therefore, the molecular structure of the antiscalant including the number of functional groups should also be considered.<sup>37</sup> For example, it has been reported that an antiscalant with five phosphonate functional groups is more effective that a tetraphosphonate inhibitor in inhibiting calcite mineralization.<sup>38</sup>

Our results revealed that both increasing the HEMPA concentration and the pH of the electrolyte delayed the gypsum crystallization process (Fig. 2 and 3). At pH ~ 4, where HEMPA with two phosphonate groups and one hydroxyl functional group was slightly deprotonated, increasing the concentration of HEMPA from 10 ppm to 70 ppm enhanced the amount of additive molecules available to complex with Ca<sup>2+</sup> ions in the solution. This resulted in a decrease in the gypsum crystallization kinetics. This notable effect was also observed in the presence of 50 ppm or 70 ppm HEMPA where a low amount of gypsum crystals formed and the turbidity plots did not reach 100%. A decrease in the turbidity of barium sulfate in the presence of nitrilotriacetic acid was also noted.<sup>39</sup> It should also be remarked that the turbidity plots reported in the presence of 10 ppm or 30 ppm HEMPA (at pH ~ 4) showed development trends similar to those obtained with carboxylic acids<sup>40</sup> or alkaline earth cations.41

On the other hand, increasing the solution pH to ~7 further deprotonated HEMPA and enhanced its antiscaling performance (Fig. 3). This is because, at a high pH value of ~7, deprotonated HEMPA molecules strongly chelated with Ca<sup>2+</sup> which reduced the activity of Ca<sup>2+</sup> ion and CaSO<sub>4</sub><sup>0</sup> ion pairs in the solution.

The observed decrease in the consumption of Ca<sup>2+</sup> during gypsum formation due to an increase in the concentration of HEMPA and the solution pH further revealed the necessity of controlling these two parameters in mitigating gypsum scaling (Table 1). This is in agreement with other findings where variations in the concentration of antiscalants such as phosphates<sup>42</sup> and polycarboxylates<sup>43</sup> together with the solution pH<sup>36</sup> affected the precipitation of gypsum crystals.

4.1.2. Surface adsorption/structural incorporation. It has been demonstrated that some additives adsorb on a growing crystal by making strong bonds with the cations present on special surface planes.44 For example, it has been verified that bisphosphonates such as zoledronate which have a high affinity for Ca<sup>2+</sup> ions adsorb onto the (001) planes of a growing calcium phosphate crystal.45 The adsorption of HEDP as an amino bisphosphonate compound onto hydroxyapatite and its crystal growth inhibition effects have also been reported.46 In addition, deprotonated additives can totally block the crystal growth process by binding onto the steps and kink sites of a growing crystal and covering a few percent of the mineral surface.<sup>47</sup> During this process, the adsorbed molecules might become trapped in the fast growing minerals. 48 The adsorption of fluorescent-tagged HEDP on the kink sites of gypsum crystals was observed using a fluorescent microscope. 49 Moreover, the additives can adsorb on the forming nuclei and prevent them from reaching the critical size. Hence, the nuclei get dissolved and the inhibitor molecules will have opportunities to adsorb on other nuclei.51

In the 10 ppm HEMPA containing solution (at pH  $\sim$  4), there was not a sufficient amount of deprotonated HEMPA molecules to adsorb on all the forming nuclei and prevent them from growing. Hence, a considerable amount of gypsum crystals quickly precipitated during which the HEMPA molecules became trapped in the solids. This caused a decrease in the concentration of HEMPA in the solution (Fig. 4). It is also worth mentioning that in this system, due to the low concentration of HEMPA with respect to the high amount of gypsum crystals formed in the solution, no P was detected by XPS analysis (Table 2). In the case of the 30 ppm HEMPA containing solution, although the concentration of the tested additive was relatively high to delay the crystallization process via the chelation effect, there were not enough HEMPA molecules in the solution to adsorb onto the forming nuclei and fully inhibit gypsum formation. Therefore, after a while (induction time), gypsum crystals formed in the solution and the turbidity graph developed to reach 100%. During this phenomenon, the HEMPA molecules adsorbed onto and incorporated into the growing crystals which resulted in a decrease in the tested additive concentration in the electrolyte (Fig. 4 and 6; Table 2).

The bright field and dark field TEM images (Fig. S5†) further show that the gypsum crystals formed without and with 30 ppm HEMPA were inhomogeneous. Although the reason for the observed inhomogeneity is not clear and needs further investigation, it might be due to the incorporation of Na, Cl and/or HEMPA molecules into the synthesized crystals. Moreover, the detected P peak in Fig. 10 confirms the association of HEMPA with the precipitated solids. Similarly, the incorporation of alendronate as a bisphosphonate into hydroxyapatite crystals up to 7 wt% has been illustrated.<sup>50</sup> The association of other elements such as cadmium,<sup>52</sup> or arsenic<sup>53</sup> with gypsum has also been observed.

It should also be considered that in the presence of 50 ppm or 70 ppm HEMPA, a high amount of additive molecules was available to adsorb onto the forming nuclei and prevent them from growing. Therefore, the turbidity did not reach 100% (Fig. 2 and Table 2).

At pH ~ 7, HEMPA was highly deprotonated but its concentration in the 10 ppm HEMPA containing system was still not enough to adsorb on all the emerging nuclei and therefore fully stop the crystallization process. Thus, after the induction time, gypsum crystals nucleated and grew which was accompanied by a gradual decrease in the concentration of HEMPA in the solution (Fig. 5). In this system, when the turbidity reached 55%, the amount of deprotonated HEMPA decreased to about 5 ppm so that the gypsum crystals could easily form and the turbidity abruptly reached 100%.

Meanwhile, the HEMPA concentration further decreased until it dropped to 0.5 ppm after 240 min (Table 1). Indeed, in this system the decrease in the HEMPA concentration over time clearly illustrates the association (i.e., surface adsorption and structural incorporation) of HEMPA with gypsum crystals (Table 2). In terms of the other tested concentrations (at pH ~ 7), the deprotonated additive molecules significantly adsorbed on the forming nuclei and did not allow them to reach the critical size. Hence, no induction time was measured.

In other literature reports, a sharp increase in the turbidity development plots when polyphosphonate<sup>30</sup> or polycarboxylate<sup>54</sup> antiscalants were utilized to inhibit gypsum precipitation has been observed.

Here it is worth noting that the association of an antiscalant with a gypsum mineral occurs through the formation of some calcium-additive compounds such as calcium phosphate. 55,56 Due to their high hydration energy, calcium ions in the gypsum structure are covered by water molecules, hence, the additive molecules adsorb onto gypsum crystals via a chemisorption mechanism called "ligand-exchange" adsorption.55 During this irreversible phenomenon the hydroxyl groups linked to the structural calcium ions of gypsum are replaced by the additive functional groups.<sup>57</sup> A similar mechanism has been reported for the adsorption of phosphonates on growing calcite crystals.58

#### 4.2. Morphological modification

It is well-known that the adsorption of some additives onto forming crystals inhibits them from growing along a particular direction.<sup>54</sup> For example, polymeric additives usually adsorb onto the tips of gypsum crystals and stop the crystal growth along the c direction.<sup>54</sup> In another research, Boanini et al., demonstrated that zoledronate can modify the morphology of a hydroxyapatite crystal.<sup>59</sup>

In the absence of HEMPA, the vacuum-filtered solids had a thin, broad and elongated morphology which was due to the high supersaturation of the solution. This morphology is different from the needle one previously obtained at a lower supersaturation.40 The significant effect of solution supersaturation on the morphology of gypsum crystals has been emphasized by others.<sup>60</sup>

At pH  $\sim$  4, the deprotonation degree of HEMPA was low. Hence, in the 10 ppm HEMPA containing solution, there were not enough deprotonated molecules to associate with the fast growing crystals and prevent them from growing. Therefore, in comparison with the thin gypsum crystals with even tips, the presence of 10 ppm HEMPA slightly thickened the final solids (Fig. 7a and b). However, the crystals produced in the presence of 30 ppm HEMPA were shorter and thicker with uneven tips where macro-steps were apparent (Fig. 8). This is because in the 30 ppm containing solution, a relatively high amount of additive molecules was present which adsorbed on the forming solids and changed their morphology (Fig. 7c and S4†). A similar phenomenon was observed when some acrylic polymers adsorbed on growing gypsum crystals and yielded final solids with uneven tips.<sup>61</sup>

When the concentration of HEMPA was further increased to 50 ppm or 70 ppm, there was a high amount of additive molecules in the solution to associate with the forming crystals. Therefore, the final solids had irregular shapes and were almost tiny (Fig. 7d and e).

At pH  $\sim$  7, where gypsum crystals just precipitated in the 10 ppm HEMPA amended solution, most of the filtered gypsum crystals just precipitated after 150 min (i.e., when HEMPA was almost depleted from the solution). Hence, the final gypsum crystals had about 90 min to nucleate and grow. Thus, the final products were very tiny (Fig. 7f). The variations in the XRD peak intensity ratio due to the morphological changes further confirm the morphological changes and the suggested mechanisms (Fig. 9). Similarly, the adsorption of carboxylic acid as an additive onto bassanite (another calcium sulfate phase; CaSO<sub>2</sub>·1/2H<sub>2</sub>O) has been demonstrated.<sup>62</sup>

### 5. Conclusion

In this research, the effects of HEMPA as an industrial antiscalant on the formation of gypsum crystals were quantitatively documented. Based on the results, the concentration of the additive and the solution pH affected the gypsum formation kinetics and hence should be considered as two main parameters by controlling which gypsum scaling can be mitigated. Furthermore, by increasing the amount of additive molecules in the solution and their deprotonation degree, HEMPA could form strong complexes with the crystal forming cations in the solution and prevent them from being used during gypsum crystallization. In addition, HEMPA adsorbed on crystals and incorporated into them, which modified the morphology of gypsum crystals from big and thin needles synthesized in the blank system to tiny particles produced with 70 ppm HEMPA (at pH  $\sim$  4). It should also be highlighted that HEMPA has the potential to be used as a gypsum antiscalant but this additive should be added to the system at particularly high concentrations (e.g., more than 10 ppm at pH  $\sim$  7), otherwise gypsum crystals will nucleate and grow which will be accompanied by a decrease in the concentration of the antiscalant in the solution. If the concentration of the dissolved antiscalant falls below a certain amount (e.g. 5 ppm in the case of HEMPA at pH  $\sim$  7), then new gypsum crystals will quickly form which will clog the pipelines and membranes used in different industries.

### Conflicts of interest

There are no conflicts to declare.

## Acknowledgements

This study was supported by the University of Tabriz.

## References

- 1 M. Mpelwa and S.-F. Tang, Pet. Sci., 2019, 16, 830-849.
- 2 G. A. Moldoveanu and V. G. Papangelakis, Hydrometallurgy, 2015, 157, 133-139.
- 3 L. Madhura, S. Kanchi, M. I. Sabela, S. Singh and K. Bisetty, Environ. Chem. Lett., 2018, 16, 343-365.
- 4 J. Jamero, S. J. Zarrouk and E. Mroczek, Geothermics, 2018, 72, 1-14.
- 5 Q. Liu, G.-R. Xu and R. Das, Desalination, 2019, 468, 114065.
- 6 M. S. Kamal, I. Hussein, M. Mahmoud, A. S. Sultan and M. A. Saad, J. Pet. Sci. Eng., 2018, 171, 127-139.
- 7 Z. Mohammadi and M. Rahsepar, J. Alloys Compd., 2019, 770, 669-678.
- 8 Z. Cao, Y. Hu, H. Zhao, B. Cao and P. Zhang, Water Res., 2022, 118945.
- 9 S. L. Wolf, K. Jähme and D. Gebauer, CrystEngComm, 2015, 17, 6857-6862.
- 10 E. D. Athanasopoulos, E. Armakola, P. G. Koutsoukos and K. D. Demadis, CrystEngComm, 2018, 20, 6589-6601.
- 11 T. Radomirovic, M. I. Ogden, A. L. Rohl and F. Jones, CrystEngComm, 2019, 21, 807-815.
- 12 A. P. Bayuseno, D. S. Perwitasari, S. Muryanto, M. Tauviqirrahman and J. Jamari, Heliyon, 2020, 6, e03533.
- 13 S. Hatte and R. Pitchumani, Soft Matter, 2022, 18, 3403-3411
- 14 X. Huang, C. Li, K. Zuo and Q. Li, Environ. Sci. Technol., 2020, 54, 15395-15404.
- 15 A. Van Driessche, T. Stawski and M. Kellermeier, Chem. Geol., 2019, 530, 119274.
- 16 M. Oshchepkov, V. Golovesov, A. Ryabova, A. Redchuk, S. Tkachenko, A. Pervov and K. Popov, Crystals, 2020, 10, 309.
- 17 S. Reigl, A. E. Van Driessche, J. Mehringer, S. Koltzenburg, W. Kunz and M. Kellermeier, CrystEngComm, 2022, 24, 1529-1536.
- 18 A. Matin, F. Rahman, H. Z. Shafi and S. M. Zubair, Desalination, 2019, 455, 135-157.
- 19 Y. Yu, H. Jin, P. Meng, Y. Guan, S. Shao and X. Chen, Sep. Purif. Technol., 2018, 191, 216-224.
- 20 J. F. Adams and V. G. Papangelakis, Can. Metall. Q., 2000, 39, 421-432.
- 21 C. Ruiz-Agudo, E. Ruiz-Agudo, A. Burgos-Cara, C. V. Putnis, A. Ibáñez-Velasco, C. Rodriguez-Navarro and A. Putnis, CrystEngComm, 2016, 18, 2830-2842.
- 22 C. Ruiz-Agudo, C. V. Putnis, A. Ibañez-Velasco, E. Ruiz-Agudo and A. Putnis, CrystEngComm, 2016, 18, 5744-5753.
- 23 M. A. Kelland, Ind. Eng. Chem. Res., 2011, 50, 5852-5861.
- 24 M. K. Jensen and M. A. Kelland, J. Pet. Sci. Eng., 2012, 94, 66-72.
- 25 A. Baynton, B. D. Chandler, F. Jones, G. Nealon, M. I. Ogden, T. Radomirovic, G. K. Shimizu and J. M. Taylor, CrystEngComm, 2011, 13, 1090-1095.
- 26 P. G. Klepetsanis, P. G. Koutsoukos and Z. Amjad, in Advances in Crystal Growth Inhibition Technologies, ed. Z. Amjad, Springer, New York, 1st edn, 2002, ch. 10, pp. 139-149.

27 Z. Amjad, R. Landgraf and J. Penn, Int. J. Corros. Scale Inhib., 2014, 3, 35-47.

- 28 E. Akyol, Ö. Doğan and M. Öner, in Mineral Scales in Biological and Industrial Systems, ed. Z. Amjad, CRC press, New York, 1st edn, 2013, ch. 4, pp. 61-76.
- 29 A. G. Reiss, I. Gavrieli and J. Ganor, Desalination, 2020, 496, 114638.
- 30 T. Rabizadeh, C. L. Peacock and L. G. Benning, Ind. Eng. Chem. Res., 2020, 59, 14970-14980.
- 31 J. MacAdam and P. Jarvis, in Mineral Scales and Deposits: Scientific and Technological Approaches, ed. Z. Amjad and K. D. Demadis, Elsevier, Amsterdam, 1st edn, 2015, ch. 1, pp. 3-47.
- 32 T. Tong, A. F. Wallace, S. Zhao and Z. Wang, J. Membr. Sci., 2019, 579, 52-69.
- 33 M. Prisciandaro, E. Olivieri, A. Lancia and D. Musmarra, Ind. Eng. Chem. Res., 2006, 45, 2070-2076.
- 34 W. Yu, D. Song, W. Chen and H. Yang, Water Res., 2020, 183, 115985.
- 35 S. A. Ali, I. Y. Yaagoob, A. A. Al-Taq, H. A. Al-Muallem and M. A. Mazumder, Desalination, 2022, 531, 115728.
- 36 Y. O. Rosenberg, I. J. Reznik, S. Zmora-Nahum and J. Ganor, Desalination, 2012, 284, 207-220.
- 37 C. B. Chew and R. Mat, Chem. Eng. Trans., 2015, 45, 1471-1476.
- 38 M. Xia and C. Chen, Int. J. Environ. Sci. Dev., 2015, 6, 300.
- 39 F. Jones, A. Oliveira, A. L. Rohl, M. I. Ogden and G. M. Parkinson, CrystEngComm, 2006, 8, 869-876.
- 40 T. Rabizadeh, C. L. Peacock and L. G. Benning, Mineral. Mag., 2014, 78, 1465-1472.
- 41 T. Rabizadeh, T. M. Stawski, D. J. Morgan, C. L. Peacock and L. G. Benning, Cryst. Growth Des., 2017, 17, 582-589.
- 42 H. A. El Dahan and H. S. Hegazy, Desalination, 2000, 127, 111-118.
- 43 K. Cao, Y. Zhou, G. Liu, H. Wang and W. Sun, J. Appl. Polym. Sci., 2014, 131, 40193-40202.
- 44 J. Chung, I. Granja, M. G. Taylor, G. Mpourmpakis, J. R. Asplin and J. D. Rimer, *Nature*, 2016, **536**, 446–450.
- 45 A. Bigi and E. Boanini, J. Funct. Biomater., 2018, 9, 6-24.
- 46 A. Zieba, G. Sethuraman, F. Perez, G. H. Nancollas and D. Cameron, Langmuir, 1996, 12, 2853-2858.
- 47 W. H. Leung and G. H. Nancollas, J. Cryst. Growth, 1978, 44, 163-167.
- 48 J. Kushnir, Geochim. Cosmochim. Acta, 1980, 44, 1471-1482.
- 49 M. Oshchepkov, S. Kamagurov, S. Tkachenko, A. Ryabova and K. Popov, ChemNanoMat, 2019, 5, 586-592.
- 50 E. Boanini, M. Gazzano, K. Rubini and A. Bigi, Adv. Mater., 2007, 19, 2499-2502.
- 51 S. Liu and G. Nancollas, J. Colloid Interface Sci., 1975, 52, 593-601.
- 52 G. J. Witkamp and G. M. Van Rosmalen, J. Cryst. Growth, 1991, 108, 89-98.
- 53 D. Zhang, Z. Yuan, S. Wang, Y. Jia and G. P. Demopoulos, J. Hazard. Mater., 2015, 300, 272-280.
- 54 T. Rabizadeh, D. J. Morgan, C. L. Peacock and L. G. Benning, Ind. Eng. Chem. Res., 2019, 58, 1561-1569.

55 M. Weijnen and G. Van Rosmalen, J. Cryst. Growth, 1986, 79, 157-168.

- 56 E. Akyol, M. Oner, E. Barouda and K. D. Demadis, Cryst. Growth Des., 2009, 9, 5145-5154.
- 57 G. Zhang and T. Yu, Coordination adsorption of anions, in Chemistry of Variable Charge Soils, ed. T. Yu, Oxford University Press, New York, 1997, pp. 175-218.
- 58 A. T. Kan, G. Fu and M. B. Tomson, J. Colloid Interface Sci., 2005, 281, 275-284.
- 59 E. Boanini, M. Gazzano and A. Bigi, J. Phys. Chem. C, 2012, 116, 15812-15818.
- 60 E. A. Abdel-Aal, M. M. Rashad and H. El-Shall, Cryst. Res. Technol., 2004, 39, 313-321.
- 61 D. Montagnino, E. Costa, F. Massaro, G. Artioli and Aquilano, Cryst. Res. Technol., 2011, 1010-1018.
- 62 F. Li, J. Liu, G. Yang, Z. Pan, X. Ni, H. Xu and Q. Huang, J. Cryst. Growth, 2013, 374, 31-36.